Port-Controlled Phasor Hamiltonian Modeling and IDA-PBC Control of Solid-State Transformer

Ragini V. Meshram, Monika Bhagwat, Shubhangi Khade, Sushama R. Wagh, Aleksandar M. Stanković, and Navdeep M. Singh

***Abstract*— This paper presents an application of interconnection and damping assignment passivity-based control (IDA-PBC) principle to the port-controlled phasor Hamiltonian (PCPH) model of solid-state transformer (SST) (comprising of three stages, namely, ac/dc rectifier, dual active bridge converter, and dc/ac inverter). A PCPH model of SST is established for each individual stages using dynamic phasor concept. In comparison with other PBC approaches, IDA-PBC offers an additional degree of freedom to solve the partial differential equations. According to the target of the controller design at each stage, the desired equilibrium point of the system is obtained. The closed-loop system performance achieves regulation of constant output dc-bus voltage and unity input power factor. Large-signal simulation results for the full system validate the simplifications introduced to obtain the controller and verify the proposed controller. Robustness of the controller is demonstrated with 20% load disturbance and 10% input disturbance. For validation of the proposed approach and its effectiveness, hardware-in-loop simulation is carried out using Opal-RT and dSPACE simulators.**

***Index Terms*— dSPACE, dynamic phasors (DPs), hardware in loop (HIL), Opal-RT, passivity-based control (PBC), port-controlled Hamiltonian (PCH), solid-state transformer (SST).**

I. Introduction

SOLID-state transformers (SST) were first proposed in FREEDM system vision [1] as a versatile, highly flexible alternative to conventional transformers. SST is one of the emerging power electronic converters, which offers reactive power support for the grid, better power quality, current limiting, management of distributed storage devices, and a regulated dc bus. In addition, it can provide active filtering to the load side, such that the load is isolated from momentary sags, swells, and harmonics on the ac grid. There are several topologies suggested for SSTs in [2]–[4] but most being evaluated today are based around the idea of bidirectional dc/dc dual active bridge (DAB) converter. SST consists of three stages: an ac/dc rectifier, a dc/dc DAB converter, and a dc/ac inverter, as shown in Fig. 1. The bidirectional power flow capability of the SST provides possibilities to feed locally generated power back to the grid. Furthermore, the low-voltage dc (LVdc) link can provide a dc bus to which photovoltaic panels, energy-storage devices, or electric-vehicle chargers can be connected. These additional features and flexibility provide a platform with which to build the future smart-grid infrastructure. For a complex power electronic system simulation, the switching model requires very short time steps and results in long simulation times. Average models allow much faster simulation and reduce memory requirement when compared with the detailed switching models. However, the switching ripple present in the state of power converters is not captured by standard average models. This problem is addressed using the dynamic phasor (DP) model based on generalized averaging method, which is Fourier series averaging method initially proposed in [5], in which time-varying signal is approximated by zeroth and higher order harmonic coefficients called DPs. This is essentially a frequency domain analysis method as explained in [6] and [7] in which Fourier coefficients are time varying as the integration interval (window) slides over the actual waveform. Compared with other time-domain modeling techniques, the DP models offer a number of advantages over conventional methods. This is due to the fact that the oscillating waveforms of ac circuits become constant or slowly varying in the DP domain and different frequency components can be handled separately with convenience. This property of DPs allows large step sizes in numerical simulations, and makes simulation potentially faster than conventional time-domain models under both balanced and unbalanced conditions [8]. The DP technique has been widely implemented in modeling electronic converters, and some of the key references in the application of DP include [9]–[11].

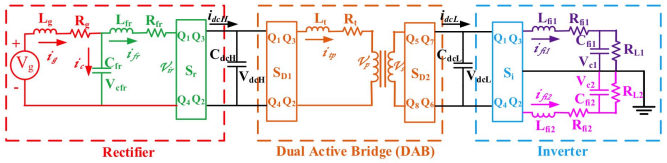

Fig. 1. SST.

The control objectives of power electronics converters include output regulation/tracking, internal variable dynamics compensation, and so on. The dynamic modeling and control of DAB is discussed in [10], [12], and [13] with a linear

Manuscript received August 10, 2016; revised March 10, 2017; accepted October 2, 2017. Date of publication November 8, 2017; date of current version December 12, 2018. Manuscript received in final form October 7, 2017. Recommended by Associate Editor B. Pal. *(Corresponding author: Ragini V. Meshram.)*

R. Meshram, M. Bhagwat, S. R. Wagh, and N. M. Singh are with the Electrical Engineering Department, Veermata Jijabai Technological Institute, Mumbai 400031, India (e-mail: raginimeshram18@gmail.com).

S. Khade is with the Trinity College, SPPU University, Pune 411007, India.

A. M. Stanković is with the Electrical Engineering and Computer Science Department, Tufts University, Medford, MA 02155 USA.

This paper has supplementary downloadable material available at http://ieeexplore.ieee.org, provided by the author. The material includes a video on hardware-in loop implementation of IDA-PBC control of solid state transformer. The total size of the video is 205 MB. Contact raginimeshram18@gmail.com for further questions about this work.

Color versions of one or more of the figures in this paper are available online at http://ieeexplore.ieee.org.

Digital Object Identifier 10.1109/TCST.2017.2761866

control. In traditional control strategies of SST, a time-domain simulation analysis is done in [2] with a two-loop cascaded control structure. A control strategy for averaged model and stability analysis of SST is discussed in [4] and [14].

In the nonlinear control theory, port-controlled Hamiltonian (PCH) control based on energy shaping has attracted considerable attention [15]–[19]. The main characteristic of the method is that the system has a PCH structure and the Hamilton function, which is the same as Lyapunov function for stability analysis. PCH systems are a natural way of representing a networked physical system in terms of its energy exchange with the environment through ports [20]. In this paper, with the concept of DP, a port-controlled phasor Hamiltonian (PCPH) structure is formed to design nonlinear controller. This PCPH structure is obtained by applying PCH structure on DP-based model. A passivity-based control (PBC) tends to offer advantages in robustness compared with linear control [21]–[25].

Interconnection and damping assignment-passivity-based control (IDA-PBC) is a general method for designing high-performance nonlinear controllers for systems described by port-Hamiltonian models. IDA-PBC has been proposed in [26] as a control technique based on energy balancing. This method designs a controller that achieves stabilization by rendering the system passive with respect to a desired storage function and injecting damping. The development of IDA-PBC control law via modification in interconnection and damping matrices for rectifier is discussed in [21]–[23] and [27] and control law for inverter is derived in [28]–[30]. The main contribution of this paper is to derive IDA-PBC control law for each stage of SST using the PCPH model.

The contributions of this paper can be listed as follows.

1) First time PCPH model is developed for SST.
2) First time PCPH model is used for control design and a nonlinear IDA-PBC is applied on the PCPH model of SST to address the voltage regulation issues because of intermittent nature of renewable sources.
3) For validation of the effectiveness of the proposed approach, hardware-in-loop (HIL) simulation is carried out using Opal-RT and dSPACE simulators, where Opal-RT module mimics the plant and dSPACE is the controller.

This paper is organized as follows. The modeling of rectifier, DAB, and inverter in PCPH form will be presented in Section II. Section III explains the execution of IDA-PBC technique to generate control law for individual stages of SST. Section IV presents the results and validation of the model with simulation waveforms. In Section V, HIL implementation is described with architecture and experimental results. Finally, Section VI states the conclusion and future scope for further improvements.

II. Port-Controlled Phasor Hamiltonian Formation of SST

In this section, PCPH formation of SST is developed by applying PCH modeling technique to a DP model of SST. The detailed time-domain model and its DP-based model are adopted from [11] and are provided in Appendix A. Various variables used in PCPH formation are listed in Appendix B.

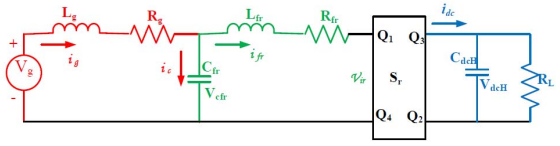

Fig. 2. Schematic of rectifier model.

A. PCPH Formation of Rectifier Stage

The topology of rectifier consists of a single H-Bridge with an input LCL filter represented in Fig. 2. Rectifier circuit includes grid inductor L_g, grid resistance R_g, filter resistance $R_{\rm fr}$, filter inductance $L_{\rm fr}$, filter capacitor $C_{\rm fr}$, HVdc link capacitor $C_{\rm dcH}$, $i_L = (V_{\rm dcH}/R_L)$ is load current, and S_r is a rectifier switching function. $V_g(t) = E\sin(\omega_o t)$ is ac grid voltage source at the rectifier with amplitude E and angular frequency $\omega_o = 2\pi f$.

The control objectives for this rectifier are as follows.

1) The dc value of output voltage should equal the desired constant value $V^d_{\rm dcH}$.
2) The power factor for converter should equal one. This means that, in steady state, the inductor current (λ_g/L_g) follows a sinusoidal signal with the same frequency and phase as the ac grid voltage source, that is:

$$\lambda^*_g(t) = L_g I_d \sin(\omega_o t) \tag{1}$$

where I_d is approximate constant value fulfilling the above objective and depends on variable $i_L(t)$. From the condition stated in [31] as input active power must be equal to the output active power, I_d can be written as

$$I_d = \frac{E}{2(R_g + R_{\rm fr})} - \sqrt{\frac{E^2}{4(R_g + R_{\rm fr})^2} - \frac{2V^d_{\rm dcH} i_L}{(R_g + R_{\rm fr})}}. \tag{2}$$

The useful variable transformation as $\mu_r(t) = -S_r(t) q_{\rm dcH}(t)$ and $z_{\rm dcH} = (1/2) q^2_{\rm dcH}$, which linearizes and decouples above dynamical equations.

The DP concept can be used for harmonic analysis, as [32] points out that the DP model is a powerful tool to explore the cyclic properties of switching systems with analysis of higher order harmonic coefficients. The nonuniform convergence of the Fourier series expansion of the system over a given time window is described in [33], along with derivation of the conditions for the existence of the solution in phasor systems.

With reference to DP coefficient in [10], the new energy-based state variables with DPs are considered in PCPH formation, which are defined as $x_r = [x_{r1}\ x_{r2}\ x_{r3}\ x_{r4}\ x_{r5}\ x_{r6}\ x_{r7}]$

$$\begin{aligned}
x_{r1} &= \langle \lambda_g \rangle^R_1 = Lg \langle i_g \rangle^R_1, \quad x_{r2} = \langle \lambda_g \rangle^I_1 = Lg \langle i_g \rangle^I_1 \\
x_{r3} &= \langle \lambda_{\rm fr} \rangle^R_1 = L_{\rm fr} \langle i_{\rm fr} \rangle^R_1, \quad x_{r4} = \langle \lambda_{\rm fr} \rangle^I_1 = L_{\rm fr} \langle i_{\rm fr} \rangle^I_1 \\
x_{r5} &= \langle q_{\rm cfr} \rangle^R_1 = C_{\rm fr} \langle V_{\rm cfr} \rangle^R_1, \quad x_{r6} = \langle q_{\rm cfr} \rangle^I_1 = C_{\rm fr} \langle V_{\rm cfr} \rangle^I_1 \\
x_{r7} &= \langle z_{\rm dcH} \rangle_0 = C^2_{\rm dcH} \langle V_{\rm dcH} \rangle^2_0 / 2.
\end{aligned}$$

Let control vector be defined as

$$\begin{aligned}
\mu_r &= [\mu_{r1}\ \mu_{r2}] = \left[\langle \mu_r \rangle^R_1\ \langle \mu_r \rangle^I_1 \right] \\
&= \left[-q_{\rm dcH} \langle S_r \rangle^R_1\ -q_{\rm dcH} \langle S_r \rangle^I_1 \right].
\end{aligned} \tag{3}$$

Dynamical equations are written as

$$\dot{x}_{r1} = \omega_o x_{r2} - \frac{R_g}{L_g} x_{r1} - \frac{x_{r5}}{C_{\rm fr}} \tag{4a}$$

$$\dot{x}_{r2} = -\omega_o x_{r1} - \frac{R_g}{L_g} x_{r2} - \frac{x_{r6}}{C_{\rm fr}} - \frac{E}{2} \tag{4b}$$

$$\dot{x}_{r3} = \omega_o x_{r4} - \frac{R_{\rm fr}}{L_{\rm fr}} x_{r3} + \frac{\mu_{r1}}{C_{\rm dcH}} x_{r7} + \frac{x_{r5}}{C_{\rm fr}} \tag{4c}$$

$$\dot{x}_{r4} = -\omega_o x_{r3} - \frac{R_{\rm fr}}{L_{\rm fr}} x_{r4} + \frac{\mu_{r2}}{C_{\rm dcH}} x_{r7} + \frac{x_{r6}}{C_{\rm fr}} \tag{4d}$$

$$\dot{x}_{r5} = \omega_o x_{r6} + \frac{1}{L_g} x_{r1} - \frac{1}{L_{\rm fr}} x_{r3} \tag{4e}$$

$$\dot{x}_{r6} = -\omega_o x_{r5} + \frac{1}{L_g} x_{r2} - \frac{1}{L_{\rm fr}} x_{r4} \tag{4f}$$

$$\dot{x}_{r7} = \frac{-2\mu_{r1}}{L_{\rm fr}} x_{r3} - \frac{2\mu_{r2}}{L_{\rm fr}} x_{r4} - i_L \sqrt{2x_{r7}}. \tag{4g}$$

This system can be given a PCPH form as

$$\dot{x}_r = (J_r(\mu_r) - R_r(x_r)) \frac{\partial H_r}{\partial x_r}(x_r) + g_{r1} i_L + g_{r2}. \tag{5}$$

Expanded form of (5) is shown in (6), as shown at the bottom of this page, and Hamiltonian function is stated in (7), as shown at the bottom of this page.

With the stated control objective, x_{r7} variable translates to

$$x_{r7}^* = \frac{1}{2} C_{\rm dcH}^2 \left(\langle V_{\rm dcH}^d \rangle_0 \right)^2 \tag{8}$$

and the power factor on the input ac grid side equal to one, for which DP variables can be expressed as $x_{r1}^* = x_{r3}^* = x_{r5}^* = 0$. Equilibrium points x_{r2}^*, x_{r4}^*, and x_{r6}^* can be obtained from dynamical equations stated in (4a)–(4g) as

$$x_{r2}^* = \frac{L_g}{L_{\rm fr}} x_{r4}^*, \quad x_{r4}^* = L_{\rm fr} I_d \tag{9}$$

$$x_{r6}^* = \left(-\frac{R_g}{L_g} x_{r2}^* - \frac{E}{2} \right) C_{\rm fr}. \tag{10}$$

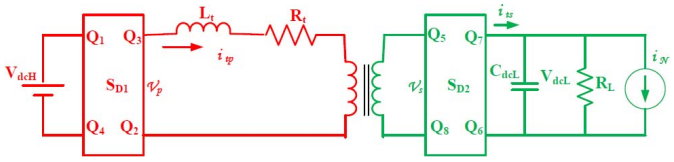

Fig. 3. Schematic of DAB model.

B. PCPH Formation of DAB

The DAB consists of a high-voltage H-Bridge, a high-frequency transformer and an LV H-bridge, as shown in Fig. 3. The rectifier controls the high-voltage side dc link voltage ($V_{\rm dcH}$) and the input ac current to be sinusoidal. The LV dc link voltage ($V_{\rm dcL}$) is regulated by the DAB converter. The current source (i_N) on the output may be of either polarity for bidirectional power flow [10]. The voltage at the input side is referred to the output side, which is represented as $V_{\rm dcH} = (V_{\rm dcL}/N)$, where N is the turns ratio of the high-frequency transformer with switching frequency f_s. Transformer leakage inductance at both windings is lumped as an equivalent inductance L_t and transformer winding resistance is lumped as an equivalent resistance R_t. The DAB topology offers zero voltage switching for all the switches, low passive component ratings, and complete symmetry of configuration that allows seamless control for bidirectional power flow. Real power flows from the bridge with leading phase angle to the bridge with lagging phase angle, the amount of power transferred being controlled by the phase angle difference, and the magnitudes of the dc voltages at the two ends as given in [10].

The control objectives for DAB is as follows. The dc value of output voltage should equal the desired constant value $V_{\rm dcL}^d$.

The change of variable is done as $z_{\rm dcL} = (1/2)(q_{\rm dcL})^2$ instead of $q_{\rm dcL}$, and control variable is also changed as $\mu_d = -S_{D2} q_{\rm dcL}$ and S_{D1} is considered constant as $\langle S_{D1} \rangle_1^R = 0$, $\langle S_{D1} \rangle_1^I = -(2/\pi)$.

$$\dot{x}_r = \underbrace{\begin{bmatrix} \frac{-R_g}{2} & \frac{\omega_o L_g}{2} & 0 & 0 & \frac{-1}{2} & 0 & 0 \\ \frac{-\omega_o L_g}{2} & \frac{-R_g}{2} & 0 & 0 & 0 & \frac{-1}{2} & 0 \\ 0 & 0 & \frac{-R_{\rm fr}}{2} & \frac{\omega_o L_{\rm fr}}{2} & \frac{1}{2} & 0 & \mu_{r1} \\ 0 & 0 & \frac{-\omega_s L_{\rm fr}}{2} & \frac{-R_f r}{2} & 0 & \frac{1}{2} & \mu_{r2} \\ \frac{1}{2} & 0 & \frac{-1}{2} & 0 & 0 & \frac{\omega_o C_{\rm fr}}{2} & 0 \\ 0 & \frac{1}{2} & 0 & \frac{-1}{2} & \frac{-\omega_o C_{\rm fr}}{2} & 0 & 0 \\ 0 & 0 & -\mu_{r1} & -\mu_{r2} & 0 & 0 & 0 \end{bmatrix}}_{(J_r(\mu_r) - R_r(x_r))} \frac{\partial H_r}{\partial x_r}(x_r) + \underbrace{\begin{bmatrix} 0 \\ 0 \\ 0 \\ 0 \\ 0 \\ 0 \\ -\sqrt{2x_{r7}} \end{bmatrix}}_{g_{r1}} i_L + \underbrace{\begin{bmatrix} 0 \\ -\frac{E}{2} \\ 0 \\ 0 \\ 0 \\ 0 \\ 0 \end{bmatrix}}_{g_{r2}} \tag{6}$$

$$H_r = \frac{1}{L_g} x_{r1}^2 + \frac{1}{L_g} x_{r2}^2 + \frac{1}{L_{\rm fr}} x_{r3}^2 + \frac{1}{L_{\rm fr}} x_{r4}^2 + \frac{1}{C_{\rm fr}} x_{r5}^2 + \frac{1}{C_{\rm fr}} x_{r6}^2 + \frac{1}{C_{\rm dcH}} x_{r7} \tag{7}$$

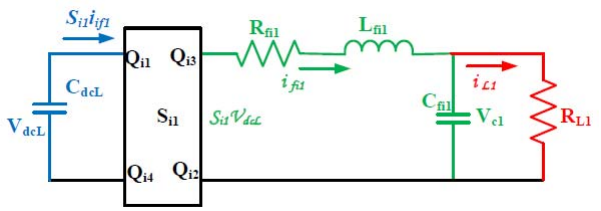

Fig. 4. Schematic of inverter model.

Let the state variables and control inputs are defined as

$$x_{\text{DAB}} = \begin{bmatrix} x_{d1} & x_{d2} & x_{d3} \end{bmatrix} = \begin{bmatrix} \langle \lambda_{\text{tp}} \rangle_1^R & \langle \lambda_{\text{tp}} \rangle_1^I & \langle z_{\text{dcL}} \rangle_0 \end{bmatrix}$$
$$\mu_d = \begin{bmatrix} \mu_{d1} & \mu_{d2} \end{bmatrix} = \begin{bmatrix} -q_{\text{dcL}} \langle S_{D2} \rangle_1^R & -q_{\text{dcL}} \langle S_{D2} \rangle_1^I \end{bmatrix}.$$

The dynamical equations are written as

$$\dot{x}_{d1} = \omega_s x_{d2} - \frac{R_t}{L_t} x_{d1} + \frac{\mu_{d1}}{C_{\text{dcL}}} x_{d3} + \langle S_{D1} \rangle_1^R \langle V_{\text{dcH}} \rangle_0 \quad (11a)$$

$$\dot{x}_{d2} = -\omega_s x_{d1} - \frac{R_t}{L_t} x_{d2} + \frac{\mu_{d2}}{C_{\text{dcL}}} x_{d3} + \langle S_{D1} \rangle_1^I \langle V_{\text{dcH}} \rangle_0 \quad (11b)$$

$$\dot{x}_{d3} = \frac{-2\mu_{d1}}{L_t} x_{d1} + \frac{-2\mu_{d2}}{L_t} x_{d2} - i_N \sqrt{2 x_{d3}}. \quad (11c)$$

This system can be given in a PCPH form as

$$\dot{x}_{\text{DAB}} = (J_{\text{DAB}}(\mu_d) - R_{\text{DAB}}) \partial H_{\text{DAB}} + g_1(x_{d3}) i_L + g_2 \langle V_{\text{dcH}} \rangle_0. \quad (12)$$

The structure and damping matrices calculation is the same as the procedure in rectifier. Hamiltonian function is defined as

$$H_{\text{DAB}} = \frac{1}{2L_t} x_{d1}^2 + \frac{1}{2L_t} x_{d2}^2 + \frac{1}{4C_{\text{dcL}}} x_{d3}^2. \quad (13)$$

The control objective is to maintain dc value of the output voltage $\langle V_{\text{dcL}} \rangle_0$ to a desired constant value $\langle V_{\text{dcL}}^d \rangle_0$. From (11a)–(11c), equilibrium points are obtained as $x_{\text{DAB}}^* = [0 \; x_{d2}^* \; x_{d3}^*]$, where $x_{d3}^* = (1/2) C_{\text{dcL}}^2 V_{\text{dcL}}^2$

$$x_{d2}^* = \sqrt{\left(\frac{\langle V_{\text{dcH}} \rangle_0 L_t}{2\pi R_t} \right)^2 + \left(\frac{\left(\langle V_{\text{dcL}}^d \rangle_0 \right)^3 L_t^2 i_N C_{\text{dcL}}^2}{4 R_t} \right)} - \left(\frac{\langle V_{\text{dcH}} \rangle_0 L_t}{\pi R_t} \right). \quad (14)$$

C. PCPH Formation of Inverter Stage

The typical structure of a single-phase inverter is presented in Fig. 4. It is composed of H-bridge with switching function S_i, which is fed by LVdc link voltage (V_{dcL}) and LC circuit is connected between inverter output and load resistance (R_L) for filtering purposes. LC filter consists of filter inductor L_{fi}, filter resistance R_{fi}, and filter capacitor C_{fi}. The aim of controller is to regulate inverter output voltage (V_{cfi}). The desired voltage is a pure sinusoidal signal with fixed angular frequency ω and amplitude V_p.

In DP model of inverter, state variables are fundamental harmonic components of inverter filter inductor current, i.e., $\langle i_{\text{fi}} \rangle_1^R$, $\langle i_{\text{fi}} \rangle_1^I$ and fundamental harmonic components of filter capacitor voltage $\langle V_{\text{cfi}} \rangle_1^R$, $\langle V_{\text{cfi}} \rangle_1^I$. The input to inverter is the zeroth harmonic component of dc bus voltage $\langle V_{\text{dcL}} \rangle_0$ and control input is first harmonic components of inverter switching function $\langle S_i \rangle_1^R$, $\langle S_i \rangle_1^I$. The state variables and control variables are defined in (15) and dynamical equations are stated in the following:

$$\begin{aligned} x_i &= \begin{bmatrix} x_{i1} & x_{i2} & x_{i3} & x_{i4} \end{bmatrix} \\ &= \begin{bmatrix} L_{\text{fi}} \langle i_{\text{fi}} \rangle_1^R & L_{\text{fi}} \langle i_{\text{fi}} \rangle_1^I & C_{\text{fi}} \langle V_{\text{cfi}} \rangle_1^R & C_{\text{fi}} \langle V_{\text{cfi}} \rangle_1^I \end{bmatrix} \\ \mu_i &= \begin{bmatrix} \mu_{i1} & \mu_{i2} \end{bmatrix} = \begin{bmatrix} \langle S_i \rangle_1^R & \langle S_i \rangle_1^I \end{bmatrix} \end{aligned} \quad (15)$$

$$\dot{x}_{i1} = \omega x_{i2} - \frac{R_{\text{fi}}}{L_{\text{fi}}} x_{i1} - \frac{1}{C_{\text{fi}}} x_{i3} + \mu_{i1} \langle V_{\text{dcL}} \rangle_0 \quad (16a)$$

$$\dot{x}_{i2} = -\omega x_{i1} - \frac{R_{\text{fi}}}{L_{\text{fi}}} x_{i2} - \frac{1}{C_{\text{fi}}} x_{i4} + \mu_{i2} \langle V_{\text{dcL}} \rangle_0 \quad (16b)$$

$$\dot{x}_{i3} = \omega x_{i4} + \frac{1}{L_{\text{fi}}} x_{i1} - \frac{1}{R_L C_{\text{fi}}} x_{i3} \quad (16c)$$

$$\dot{x}_{i4} = -\omega x_{i3} + \frac{1}{L_{\text{fi}}} x_{i2} - \frac{1}{R_L C_{\text{fi}}} x_{i4}. \quad (16d)$$

This system can be given in a PCPH form in (17) where structure and damping matrices calculation is the same as for the rectifier, and Hamiltonian function is given in (18)

$$\dot{x}_i = (J_i(x_i) - R_i(x_i)) \partial H_i + g(\mu_i) \langle V_{\text{dcL}} \rangle_0 \quad (17)$$

$$H_i = \frac{1}{2L_{\text{fi}}} x_{i1}^2 + \frac{1}{2L_{\text{fi}}} x_{i2}^2 + \frac{1}{2C_{\text{fi}}} x_{i3}^2 + \frac{1}{2C_{\text{fi}}} x_{i4}^2. \quad (18)$$

The goal of control is to regulate voltage V_{cfi} across the load around to the desired value V_{cfi}^d. From (16a)–(16d), equilibrium points are obtained as

$$x_i^* = \begin{bmatrix} x_{i1}^* & x_{i2}^* & x_{i3}^* & x_{i4}^* \end{bmatrix} \quad (19)$$

$$x_{i1}^* = 0, \quad x_{i2}^* = L_{\text{fi}} \langle i_{\text{cfi}} \rangle_1^{I^d} \quad (20)$$

$$x_{i3}^* = 0, \quad x_{i4}^* = C_{\text{fi}} \langle V_{\text{cfi}} \rangle_1^{I^d}. \quad (21)$$

III. Controller Design Using IDA-PBC Technique

The IDA-PBC was introduced in [26] to combine passivity properties of PCHS with control by interconnection and energy based control. The idea of IDA-PBC is to assign desired energy function to the closed-loop system via modification of the interconnection and dissipation matrices.

There exist two approaches to PBC: energy shaping plus damping injection and IDA-PBC. In the former, the energy function is shaped, and then, damping is injected through R matrix without modifying J matrix. On the other hand, in the latter, the interconnection matrix J and the damping matrix R are assigned, and then, the energy function is modified to the desired value. This gives additional degree of freedom to solve the partial differential equations (PDEs) [17], [34] via matching condition.

The key idea is that using Hamiltonian framework, solving the PDE associated with the energy balance equation is accomplished with an appropriate selection of the interconnection J and dissipation R matrices and the energy function H of the desired closed-loop system. The desired target closed-loop system dynamics is of form

$$\dot{x_d} = (J_d(x) - R_d(x))(\partial H_d(x))^T \quad (22)$$

where H_d is the desired Hamiltonian energy function (minimum at x^*) and $J_d = -J_d^T$ and $R_d = R_d^T \geq 0$ are desired interconnection and dissipation matrices, respectively.

To achieve stabilization of the desired equilibrium point, we impose $x^* = \arg\min H_d(x)$. The matching objective is to achieve if and only if the following PDE:

$$(J(x) - R(x))(\partial H(x))^T + g = (J_d(x) - R_d(x))(\partial H_d(x))^T \tag{23}$$

is satisfied. There is a considerable freedom in selecting J_d, R_d, and H_d to satisfy previous assumptions. For convenience, we define $H_d(x) = H(x) + H_a(x)$, $J_d(x) = J(x) + J_a(x)$, $R_d(x) = R(x) + R_a(x)$, and $g = g_1(x_7) + g_2\ V_g$

Fixing the interconnection and damping matrices as $J_d = J$ and $R_d = R$, (23) simplifies to

$$-(J(x) - R(x))(\partial H_a(x))^T + g = 0. \tag{24}$$

To confirm whether x^* is locally stable equilibrium point, it is necessary to check the following four conditions.

1) Structure Preservation: Given J_d and R_d matrices, J_a and R_a matrices can be defined by

$$J_d(x) = J(x,u) + J_a(x) = -[J(x,u) + J_a(x)]^T \tag{25}$$

$$R_d(x) = R(x,u) + R_a(x) = [R(x,u) + R_a(x)]^T \geq 0. \tag{26}$$

Then, the desired dynamics is achieved if it is possible to find functions $u\ (x)$ and $k(x) = (\partial H_a/\partial x)(x)$ satisfying

$$[(J(x,u)) + J_a(x)) - (R(x,u) + R_a(x))]k(x) = -[J_a - R_a]\frac{\partial H}{\partial x}(x) + g(x,\mu). \tag{27}$$

2) Integrability: $(\partial k_i/\partial x_j)(x) = (\partial k_j/\partial x_i)(x)$.

3) Equilibrium Condition: $(\partial H_d/\partial x)(x^*) = 0$.

4) Lyapunov Stability: $(\partial^2 H_d/\partial x^2) \mid x^* > 0$.

If the above four conditions hold, then x^* is a (locally) stable equilibrium point of the closed-loop system. The flowchart of the IDA-PBC algorithm is shown in Fig. 5, which is divided in three major parts: formation of PCPH system which is discussed in detail for individual components in Section III, desired dynamic system by (22)–(24), and IDA-PBC is designed by conditions 1–4

A. Controller Design for Rectifier

The procedural steps for the IDA-PBC controller design are shown in Fig. 5 for the rectifier stage. Defining $k(x) = (k_1, k_2, k_3, k_4, k_5, k_6, k_7)^T = (\partial H_{\text{ra}})^T$

$$0 = \frac{R_g}{2}k_1 - \frac{\omega_s L_g}{2}k_2 + \frac{1}{2}k_5 \tag{28a}$$

$$0 = -\frac{\omega_s L_g}{2}k_1 + \frac{R_g}{2}k_2 + \frac{1}{2}k_6 - \frac{E}{2} \tag{28b}$$

$$0 = \frac{R_{\text{fr}}}{2}k_3 - \frac{\omega_s L_{\text{fr}}}{2}k_4 - \frac{1}{2}k_5 - \mu_{r1}k_7 \tag{28c}$$

$$0 = \frac{\omega_s L_{\text{fr}}}{2}k_3 + \frac{R_{\text{fr}}}{2}k_4 - \frac{1}{2}k_6 - \mu_{r2}k_7 \tag{28d}$$

$$0 = -\frac{1}{2}k_1 + \frac{1}{2}k_3 - \frac{\omega_s C_{\text{fr}}}{2}k_6 \tag{28e}$$

$$0 = -\frac{1}{2}k_2 + \frac{1}{2}k_4 + \frac{\omega_s C_{\text{fr}}}{2}k_6 \tag{28f}$$

$$0 = \mu_{r1}k_3 + \mu_{r2}k_4 - i_L\sqrt{2x_{r7}}. \tag{28g}$$

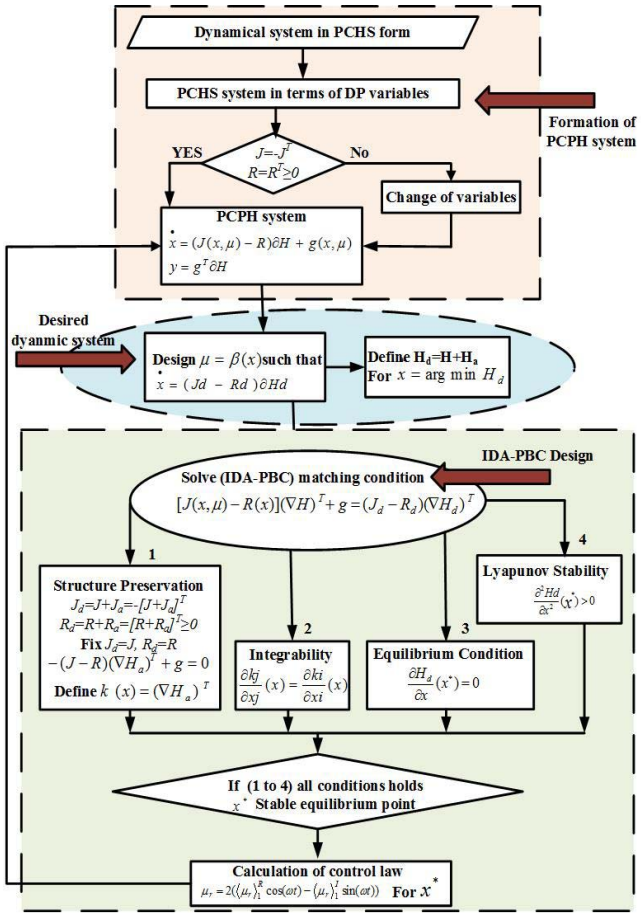

Fig. 5. Flowchart of IDA-PBC algorithm.

From (28a)–(28d), control equations are obtained as

$$\mu_{r1} = \frac{R_{\text{fr}}k_3 - \omega_s L_{\text{fr}}k_4 + R_g k_1 - \omega_s L_g k_2}{2k_7} \tag{29}$$

$$\mu_{r2} = \frac{\omega_s L_{\text{fr}}k_3 + R_{\text{fr}}k_4 - \omega_s L_g k_1 + R_g k_2 - E}{2k_7} \tag{30}$$

and replacing (29) and (30) in (28g), PDE is obtained as

$$R_{\text{fr}}(k_3^2 + k_4^2) + R_g(k_1k_3 + k_2k_4) - \omega_s L_g(k_2k_3 + k_1k_4) - Ek_4 - 2i_L\sqrt{2x_{r7}}k_7 = 0. \tag{31}$$

As control inputs μ_{r1} and μ_{r2} depends only on x_{r7}, considering $k_1 = k_1(x_{r7})$, $k_2 = k_2(x_{r7})$, $k_3 = k_3(x_{r7})$, $k_4 = k_4(x_{r7})$, $k_5 = k_5(x_{r7})$, $k_6 = k_6(x_{r7})$ and $k_7 = k_7(x_{r7})$ and consequently, using the integrability condition

$$\frac{\partial k_i}{\partial x_{rj}}(x_r) = \frac{\partial k_j}{\partial x_{ri}}(x_r). \tag{32}$$

Let $k_1 = a_1$, $k_2 = a_2$, $k_3 = a_3$, $k_4 = a_4$, $k_5 = a_5$, and $k_6 = a_6$ are constants. Then, from (31), k_7 is written as

$$k_7 = \frac{1}{2i_L\sqrt{2x_{r7}}}\big(R_{\text{fr}}(a_3^2 + a_4^2) + R_g(a_1a_3 + a_2a_4) - \omega_s L_g(a_2a_3 + a_1a_4) - Ea_4\big). \tag{33}$$

$$H_{\rm ra} = -\frac{2\sqrt{x_{r7}^*}}{C_{\rm dcH}}\sqrt{x_{r7}} - \frac{2}{L_g}x_{r2}^* x_{r2} - \frac{2}{L_{\rm fr}}x_{r4}^* x_{r4} - \frac{2}{C_{\rm fr}}x_{r6}^* x_{r6} \tag{37}$$

$$H_{\rm rd} = \frac{1}{L_g}\left(x_{r1}^2 + x_{r2}^2\right) + \frac{1}{L_{\rm fr}}\left(x_{r3}^2 + x_{r4}^2\right) + \frac{1}{C_{\rm fr}}\left(x_{r5}^2 + x_{r6}^2\right) + \frac{1}{C_{\rm dcH}}x_{r7} - \frac{2\sqrt{x_{r7}^*}}{C_{\rm dcH}}\sqrt{x_{r7}} - \frac{2}{L_g}x_{r2}^* x_{r2} - \frac{2}{L_{\rm fr}}x_{r4}^* x_{r4} - \frac{2}{C_{\rm fr}}x_{r6}^* x_{r6} \tag{38}$$

$$\frac{\partial^2 H_{\rm rd}}{\partial x_r^2}\Big|_{x_r = x_r^*} = {\rm diag}\left(\frac{2}{L_g}, \frac{2}{L_g}, \frac{2}{L_{\rm fr}}, \frac{2}{L_{\rm fr}}, \frac{2}{C_{\rm fr}}, \frac{2}{C_{\rm fr}}, \frac{1}{2C_{\rm dcH}\sqrt{x_{r7}^*}}\right) \tag{39}$$

$$\mu_{r1} = \frac{-\omega_s(L_g + L_{\rm fr})\left(-E + \sqrt{E^2 - 8i_L\langle V_{\rm dcH}^d\rangle_0(R_g + R_{\rm fr})}\right)C_{\rm dcH}\sqrt{\langle V_{\rm dcH}\rangle_0\langle V_{\rm dcH}^d\rangle_0}}{4(R_g + R_{\rm fr})\langle V_{\rm dcH}^d\rangle_0} \tag{40}$$

$$\mu_{r2} = \frac{\left(E + \sqrt{E^2 - 8i_L\langle V_{\rm dcH}^d\rangle_0(R_g + R_{\rm fr})}\right)C_{\rm dcH}\sqrt{\langle V_{\rm dcH}\rangle_0\langle V_{\rm dcH}^d\rangle_0}}{4\langle V_{\rm dcH}^d\rangle_0} \tag{41}$$

The equilibrium condition defined as

$$\partial H_{\rm rd}|_{x_r = x_r^*} = (\partial H_r + \partial H_{\rm ra})|_{x_r = x_r^*} = 0 \tag{34}$$

$$\frac{2}{L_g}x_{r1}^* + a_1 = 0, \quad \frac{2}{L_g}x_{r2}^* + a_2 = 0$$

$$\frac{2}{L_{\rm fr}}x_{r3}^* + a_3 = 0, \quad \frac{2}{L_{\rm fr}}x_{r4}^* + a_4 = 0$$

$$\frac{2}{C_{\rm fr}}x_{r5}^* + a_5 = 0, \quad \frac{2}{C_{\rm fr}}x_{r6}^* + a_6 = 0$$

$$\frac{1}{C_{\rm dcH}} + k_7(x_{r7}^*) = 0. \tag{35}$$

Since $x_{r1}^* = 0$, $x_{r3}^* = 0$, and $x_{r5}^* = 0$, hence $a_1 = 0$, $a_3 = 0$, and $a_5 = 0$, respectively, and $a_2 = -(2/L_g)x_{r2}^*$, $a_4 = -(2/L_{\rm fr})x_{r4}^*$, and $a_6 = -(2/C_{\rm fr})x_{r6}^*$. Substituting these values in (33) yields

$$k_7 = -\frac{1}{C_{\rm dcH}}\sqrt{\frac{x_{r7}^*}{x_{r7}}} \tag{36}$$

which satisfies the equilibrium condition (35). The PDE (31) is solved and $H_{\rm ra}$ is obtained as (37) shown at the top of this page.

$H_{\rm rd}$ is calculated in (38), as shown at the top of this page. To guarantee that $H_{\rm rd}$ has a minimum at $x_r = x_r^*$, $\partial H_{\rm rd} = 0$ and Hession of $H_{\rm rd}$ is always positive definite as shown in (39), as shown at the top of this page, so the minimum condition is satisfied for stability analysis. Substituting values of $k(x)$ in (29) and (30), the control law is expressed in terms of the output voltage $\langle V_{\rm dcH}\rangle_0$ is shown in (40) and (41), as shown at the top of this page. Control variable μ_r is obtained from (40) and (41) as

$$\mu_r = 2(\mu_{r1}\cos(\omega_s t) - \mu_{r2}\sin(\omega_s t)). \tag{42}$$

The control action S_r is calculated as $S_r = -(1/\sqrt{2x_{r7}})\mu_r$.

B. Controller Design of DAB

Defining $k(x) = (k_1, k_2, k_3)^T = (\partial H_{\rm DABa})^T$

$$0 = -\frac{R_t}{2}k_1 + \frac{\omega_s L_t}{2}k_2 + \mu_{d1}k_3 \tag{43}$$

$$0 = -\frac{\omega_s L_t}{2}k_1 - \frac{R_t}{2}k_2 + \mu_{d2}k_3 + \langle S_{D1}\rangle_1^I\langle V_{\rm dcH}\rangle_0 \tag{44}$$

$$0 = -\mu_{d1}k_1 - \mu_{d2}k_2 - i_N\sqrt{2x_{d3}}. \tag{45}$$

From (43) and (44), control equations are obtained as

$$\mu_{d1} = \frac{R_t k_1 - \omega_s L_t k_2}{2k_3} \tag{46}$$

$$\mu_{d2} = \frac{\omega_s L_t k_1 + R_t k_2 - 2\langle S_{D1}\rangle_1^I\langle V_{\rm dcH}\rangle_0}{2k_3}. \tag{47}$$

PDE is obtained after replacing (46) and (47) in (45) as

$$R_t\left(k_1^2 + k_2^2\right) - 2k_2\langle S_{D1}\rangle_1^I\langle V_{\rm dcH}\rangle_0 + 2i_N\sqrt{2x_{d3}}k_3 = 0. \tag{48}$$

The control inputs μ_{d1} and μ_{d2} which only depends on x_{d3}, so that take $k_1 = k_1(x_{d3})$, $k_2 = k_2(x_{d3})$, and $k_3 = k_3(x_{d3})$ and consequently, using the integrability condition, $k_1 = a_1$ and $k_2 = a_2$ are constants. Then, from (48)

$$k_3 = \frac{2k_2\langle S_{D1}\rangle_1^I\langle V_{\rm dcH}\rangle_0 - R_t\left(k_1^2 + k_2^2\right)}{2i_N\sqrt{2x_{d3}}}. \tag{49}$$

The equilibrium condition is defined by

$$\partial H_{\rm DABd}\Big|_{x_{\rm DAB} = x_{\rm DAB}^*} = (\partial H_{\rm DAB} + \partial H_{\rm DABa})\Big|_{x_{\rm DAB} = x_{\rm DAB}^*} = 0 \tag{50}$$

$$\frac{2}{L_t}x_{d1}^* + a_1 = 0, \quad \frac{2}{L_t}x_{d2}^* + a_2 = 0$$

$$\frac{1}{C_{\rm dcL}}x_{d3}^* + k_3(x_{d3}^*) = 0. \tag{51}$$

Since $x_{d1}^* = 0$, $a_1 = 0$ and $a_2 = -(2/L_t)x_{d2}^*$. Substituting these values in (49) yields

$$k_3 = -\frac{1}{C_{\rm dcL}}\sqrt{\frac{x_{d3}^*}{x_{d3}}} \tag{52}$$

which satisfies the equilibrium condition (51). The PDE (48) is solved and H_{DABa} and H_{DABd} are obtained as

$$H_{\mathrm{DABa}} = -\frac{2}{L_t}x^*_{d2}x_{d2} - \frac{2\sqrt{x^*_{d3}}}{C_{\mathrm{dcL}}}\sqrt{x_{d3}} \tag{53}$$

$$H_{\mathrm{DABd}} = \frac{1}{2L_t}x^2_{d1} + \frac{1}{2L_t}x^2_{d2} + \frac{1}{4C_{\mathrm{dcL}}}x^2_{d3} - \frac{2}{L_t}x^*_{d2}x_{d2} - \frac{2\sqrt{x^*_{d3}}}{C_{\mathrm{dcL}}}\sqrt{x_{d3}}. \tag{54}$$

To guarantee that H_{DABd} has a minimum at $x_d = x^*_d$, $\partial H_{\mathrm{DABd}} = 0$ and Hession of H_{DABd} have to obey

$$\frac{\partial^2 H_{\mathrm{DABd}}}{\partial x^2_{\mathrm{DAB}}}\Big|_{x_{\mathrm{DAB}}=x^*_{\mathrm{DAB}}} > 0$$

$$\frac{\partial^2 H_{\mathrm{DABd}}}{\partial x^2_{\mathrm{DAB}}}\Big|_{x_{\mathrm{DAB}}=x^*_{\mathrm{DAB}}} = \mathrm{diag}\left(\frac{1}{L_t}, \frac{1}{L_t}, \frac{1}{2C_{\mathrm{dcL}}\sqrt{x^*_{d3}}}\right) \tag{55}$$

which is a positive definite, hence minimum condition is satisfied. Substituting values of k_1, k_2, and k_3 in (46) and (47), the control laws is obtained in terms of V_{dcL} as

$$\mu_{d1} = \frac{-2\omega x^*_{d2}C_{\mathrm{dcL}}\langle V_{\mathrm{dcL}}\rangle_0}{\langle V^d_{\mathrm{dcL}}\rangle_0} \tag{56}$$

$$\mu_{d2} = \frac{\left(-\frac{R_t}{L_t}x^*_{d2} + \langle S_{D1}\rangle^I_1\langle V_{\mathrm{dcH}}\rangle_0\right)\langle V_{\mathrm{dcL}}\rangle_0 C_{\mathrm{dcL}}}{\langle V^d_{\mathrm{dcL}}\rangle_0}. \tag{57}$$

The control variable μ_d is obtained by

$$\mu_d = 2(\mu_{d1}\cos(\omega_s t) - \mu_{d2}\sin(\omega_s t)). \tag{58}$$

The control action S_{D2} is calculated as $S_{D2} = -(1/\sqrt{2x_{d3}})\mu_d$.

C. Controller Design of Inverter

Defining $k(x) = (k_1, k_2, k_3, k_4)^T = (\partial H_{\mathrm{ia}})^T$

$$0 = R_{\mathrm{fi}}k_1 - \omega L_{\mathrm{fi}}k_2 + k_3 + \mu_{i1}\langle V_{\mathrm{dcL}}\rangle_0 \tag{59a}$$

$$0 = \omega L_{\mathrm{fi}}k_1 - R_{\mathrm{fi}}k_2 + k_4 + \mu_{i2}\langle V_{\mathrm{dcL}}\rangle_0 \tag{59b}$$

$$0 = -k_1 + \frac{1}{R_L}k_3 - \omega C_{\mathrm{fi}}k_4 \tag{59c}$$

$$0 = -k_2 + \omega C_{\mathrm{fi}}k_3 + \frac{1}{R_L}k_4. \tag{59d}$$

From (59a) and (59b), control equations are obtained as

$$\mu_{i1} = \frac{-R_{\mathrm{fi}}k_1 + \omega L_{\mathrm{fi}}k_2 - k_3}{\langle V_{\mathrm{dcL}}\rangle_0} \tag{60}$$

$$\mu_{i2} = \frac{-\omega L_{\mathrm{fi}}k_1 + R_{\mathrm{fi}}k_2 - k_4}{\langle V_{\mathrm{dcL}}\rangle_0}. \tag{61}$$

The equilibrium condition is defined as

$$\partial H_{\mathrm{id}}|_{x_i=x^*_i} = (\partial H_i + \partial H_{\mathrm{ia}})|_{x_i=x^*_i} = 0 \tag{62}$$

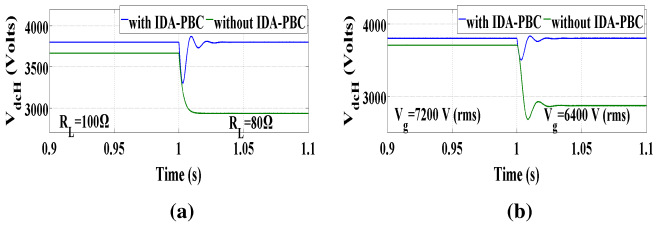

Fig. 6. Performance of rectifier with and without control. (a) Load change. (b) Input change.

k_1, k_2, k_3, and k_4 are expressed as

$$\frac{x^*_{i1}}{L_{\mathrm{fi}}} + k_1 = 0 \quad \frac{x^*_{i2}}{L_{\mathrm{fi}}} + k_2 = 0$$

$$\frac{x^*_{i3}}{C_{\mathrm{fi}}} + k_3 = 0 \quad \frac{x^*_{i4}}{C_{\mathrm{fi}}} + k_4 = 0 \tag{63}$$

$$k_3 = \frac{-x^*_{i3}}{C_{\mathrm{fi}}} = 0, \quad k_4 = \frac{-x^*_{i4}}{C_{\mathrm{fi}}} = -\langle V_{\mathrm{cfi}}\rangle^{I^d}_1$$

$$k_1 = \frac{k_3}{R_L} - \omega C_{\mathrm{fi}}k_4 = \omega C_{\mathrm{fi}}\langle V_{\mathrm{cfi}}\rangle^{I^d}_1$$

$$k_2 = \omega C_{\mathrm{fi}}k_3 + \frac{k_4}{R_L} = \frac{-\langle V_{\mathrm{cfi}}\rangle^{I^d}_1}{R_L}. \tag{64}$$

Quantities in (64) satisfy condition 3) based on power conservation $\langle V_{\mathrm{cfi}}\rangle^{I^d}_1 = R_L\langle i_{\mathrm{cfi}}\rangle^{I^d}_1$ at x^*_i, H_{ia} is

$$H_{\mathrm{ia}} = \omega C_{\mathrm{fi}}\langle V_{\mathrm{cfi}}\rangle^{I^d}_1 x_{i1} - \frac{\langle V_{\mathrm{cfi}}\rangle^{I^d}_1}{R_L}x_{i2} - \langle V_{\mathrm{cfi}}\rangle^{I^d}_1 x_{i4}. \tag{65}$$

It is seen from (67), as shown at the bottom of this page, at $x_i = x^*_i$, $\partial H_{\mathrm{id}} = 0$, and Hession of H_{id} is shown in (66) to be positive definite

$$\frac{\partial^2 H_{\mathrm{id}}}{\partial x^2_i}\Big|_{x_i=x^*_i} = \mathrm{diag}\left(\frac{1}{L_{\mathrm{fi}}}, \frac{1}{L_{\mathrm{fi}}}, \frac{1}{C_{\mathrm{fi}}}, \frac{1}{C_{\mathrm{fi}}}\right) \tag{66}$$

The control law is obtained as

$$\mu_{i1} = \frac{-R_{\mathrm{fi}}C_{\mathrm{fi}}\omega\langle V_{\mathrm{cfi}}\rangle^{I^d}_1 - \omega L_{\mathrm{fi}}\frac{\langle V_{\mathrm{cfi}}\rangle^{I^d}_1}{R_L}}{\langle V_{\mathrm{dcL}}\rangle_0} \tag{68}$$

$$\mu_{i2} = \frac{-\omega^2 L_{\mathrm{fi}}C_{\mathrm{fi}}\langle V_{\mathrm{cfi}}\rangle^{I^d}_1 - R_{\mathrm{fi}}\frac{\langle V_{\mathrm{cfi}}\rangle^{I^d}_1}{R_L} + \langle V_{\mathrm{cfi}}\rangle^{I^d}_1}{\langle V_{\mathrm{dcL}}\rangle_0}. \tag{69}$$

The control variable μ_i is obtained by

$$\mu_i = S_i = 2(\mu_{i1}\cos(\omega t) - \mu_{i2}\sin(\omega t)). \tag{70}$$

The solution of partial differential equations involved in control design procedure is summarized as follows for the rectifier.

1) Decide desired dynamics, preserving the system structure, in the form $\dot{x} = (J_d - R_D)\partial H_d$ (22), where H_d is a desired Hamiltonian function (with minimum at x^*).

$$H_{\mathrm{id}} = \frac{1}{2L_{f1}}x^2_{i1} + \frac{1}{2L_{f1}}x^2_{i2} + \frac{1}{2C_{f1}}x^2_{i3} + \frac{1}{2C_{f1}}x^2_{i4} + \omega C_{\mathrm{fi}}\langle V_{\mathrm{cfi}}\rangle^{I^d}_1 x_{i1} - \frac{\langle V_{\mathrm{cfi}}\rangle^{I^d}_1}{R_L}x_{i2} - \langle V_{\mathrm{cfi}}\rangle^{I^d}_1 x_{i4} \tag{67}$$

TABLE I
SIMULATION PARAMETERS [11]

Rectifier Parameters		
Input grid voltage RMS	V_g	7.2 kV
Grid side line resistance	R_g	36.87 Ω
Grid side line inductance	L_g	121 mH
Filter resistance	R_{fr}	11.2 Ω
Filter inductance	L_{fr}	170 mH
Filter capacitance	C_{fr}	0.04 μF
HVDC link capacitor	C_{dcH}	42 μF
DAB Parameters		
Winding resistance	R_t	0.4 Ω
Leakage inductance	L_t	250 μH
LVDC link capacitor	C_{dcL}	540 μF
DAB switching frequency	f_s	10 kHz
Inverter Parameters		
Filter resistance	R_{fi}	0.07 Ω
Filter inductance	L_{fi}	1.07 mH
Filter capacitance	C_{fi}	30 μF
Load Resistance	R_L	100 Ω

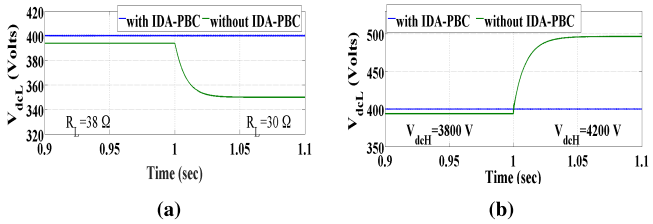

Fig. 7. Performance of DAB with and without control. (a) Load change. (b) Input change.

2) $H_d = H + H_a$, where H is given and H_a is to be designed.
3) Applying matching conditions gives PDE of the form $-(J - R)\partial H_a + g = 0$, where PDE is solved in terms of H_a (24).
4) Define vector $k = [k_1, k_2, k_3, k_4, k_5, k_6, k_7]^T = (\partial H_{\text{ra}})^T$ to get algebraic equations in terms of k [see (28a)–(28g)].
5) Using (28a)–(28g), control equations are obtained in (29) and (30).
6) Replace (29) and (30) in output voltage equation (28g), which gives PDE as (31).
7) Since the control input is dependent only on x_{r7}, all variables in vector k represented in terms of x_{r7}.
8) Assume $H_{\text{ra}} = a_1x_{r1} + a_2x_{r2} + a_3x_{r3} + a_4x_{r4} + a_5x_{r5} + a_6x_{r6} + a_7 f(x_{r7})$.
9) Use the integrability condition (32) and equilibrium condition (34) to solve for a_i and $f(x_{r7})$ as in (35) and (36) to get the required H_{ra}.

It should be noted that, if any of the key state variables are not measurable, then in case an estimator or observer design may be required. However, in this paper, the focus is to develop an energy shaping methodology for SST, where the control law is dependent only on states (e.g., x_{r7} in case of a rectifier). This is the output voltage which is typically available directly through measurements, so an estimator or observer design was not required for rectifier as well as DAB or inverter stages.

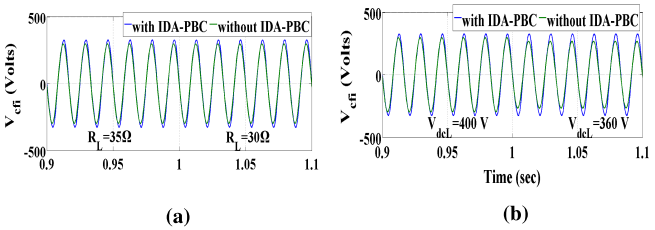

Fig. 8. Performance of inverter with and without control. (a) Load change. (b) Input change.

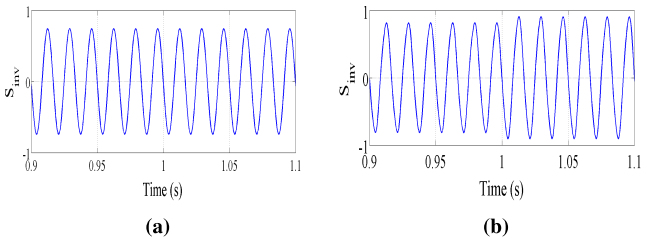

Fig. 9. Inverter switching function with and without IDA-PBC controller. (a) Uncontrolled S_i. (b) S_i with IDA-PBC control.

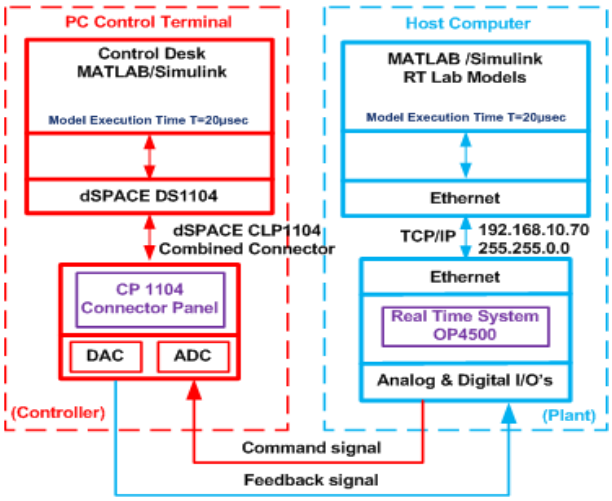

Fig. 10. HIL architecture.

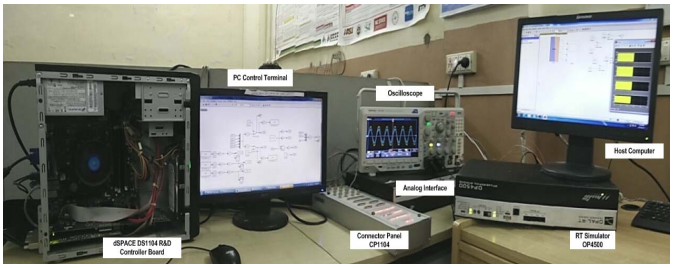

Fig. 11. HIL test bed.

IV. SIMULATION RESULTS AND VALIDATION

To verify developed IDA-PBC controller for PCPH model of SST, simulations are carried out in MATLAB/Simulink. The validation of control law is performed under the condition of load change and input change. The SST parameters used for simulation are given in Table I.

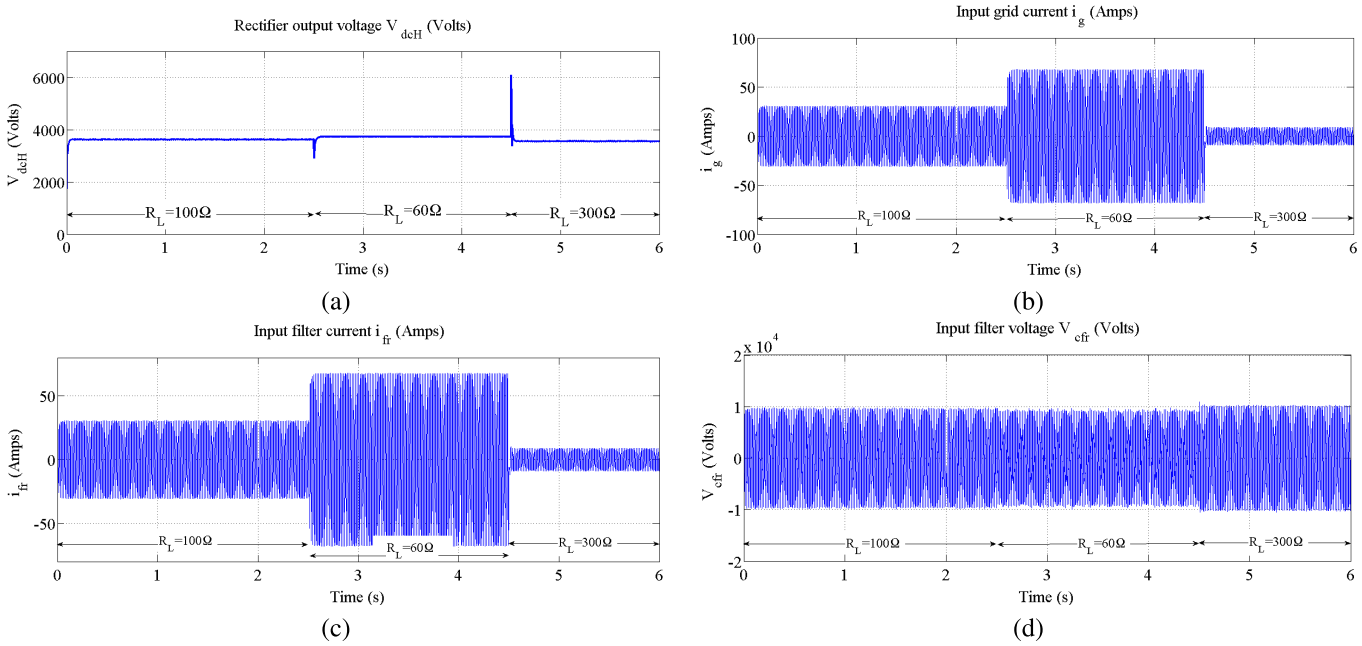

Fig. 12. HIL performance of the rectifier stage for load variations. (a) Output voltage. (b) Input grid current. (c) Input filter current. (d) Input filter voltage.

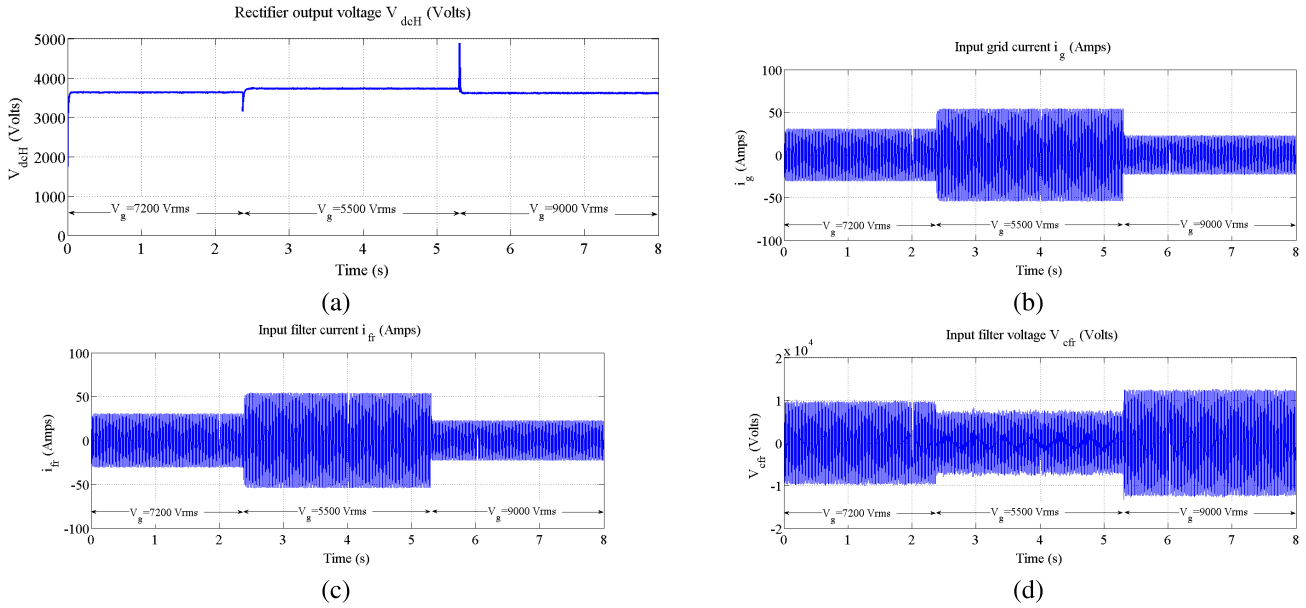

Fig. 13. HIL performance of the rectifier stage for input variations. (a) Output voltage. (b) Input grid current. (c) Input filter current. (d) Input filter voltage.

A. Load Change

In this case, 20% step change in load is considered at each stage of SST. For rectifier operation, the input grid voltage is 7200 V_{rms} and the desired value of voltage to be regulated is 3800 V. The load change condition is considered as 100 Ω for 0 sec $< t <$ 1 s and then changed to 80 Ω for 1 s $< t <$ 2 s. The output HVdc bus voltage waveform with and without IDA-PBC controller is depicted in Fig. 6(a) where we can see that system is tracking set value by varying duty ratio.

The load variation for DAB is considered as 38 Ω for 0 s $< t <$ 1 s and then changed to 30 Ω for 1 s $< t <$ 2 s. The voltage to be regulated for DAB is 400 V and input voltage given is 3800 V_{dc}. Fig. 7(a) shows the LVdc bus voltage output with and without IDA-PBC controller under load change.

The desired set value for inverter is 230 V_{rms} and load alters from 35 to 30 Ω at 1 s. The output waveforms are shown in Fig. 8(a). With designed control law, system is tracking set value with change in duty ratio.

B. Input Change

In this case, 10% of input variation occurs at each stage of SST. For rectifier stage, the load resistance is 100 Ω and

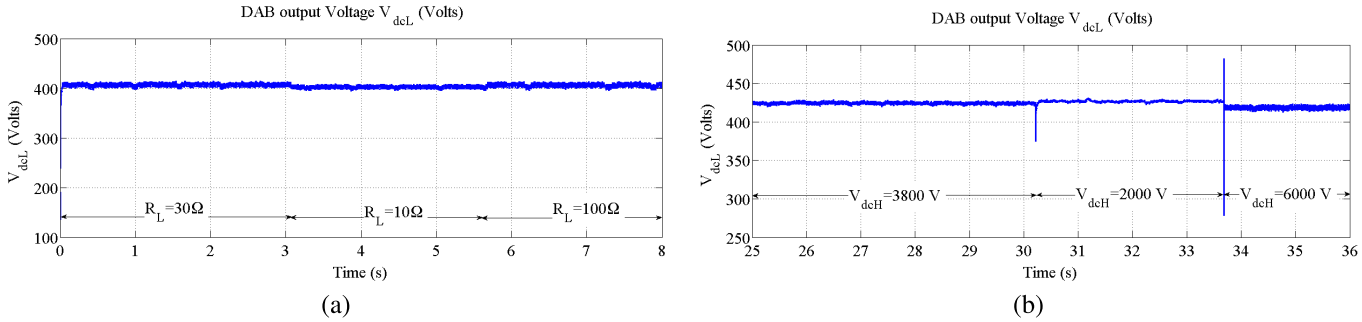

Fig. 14. HIL performance of DAB output voltage. (a) Load variations. (b) Input variations.

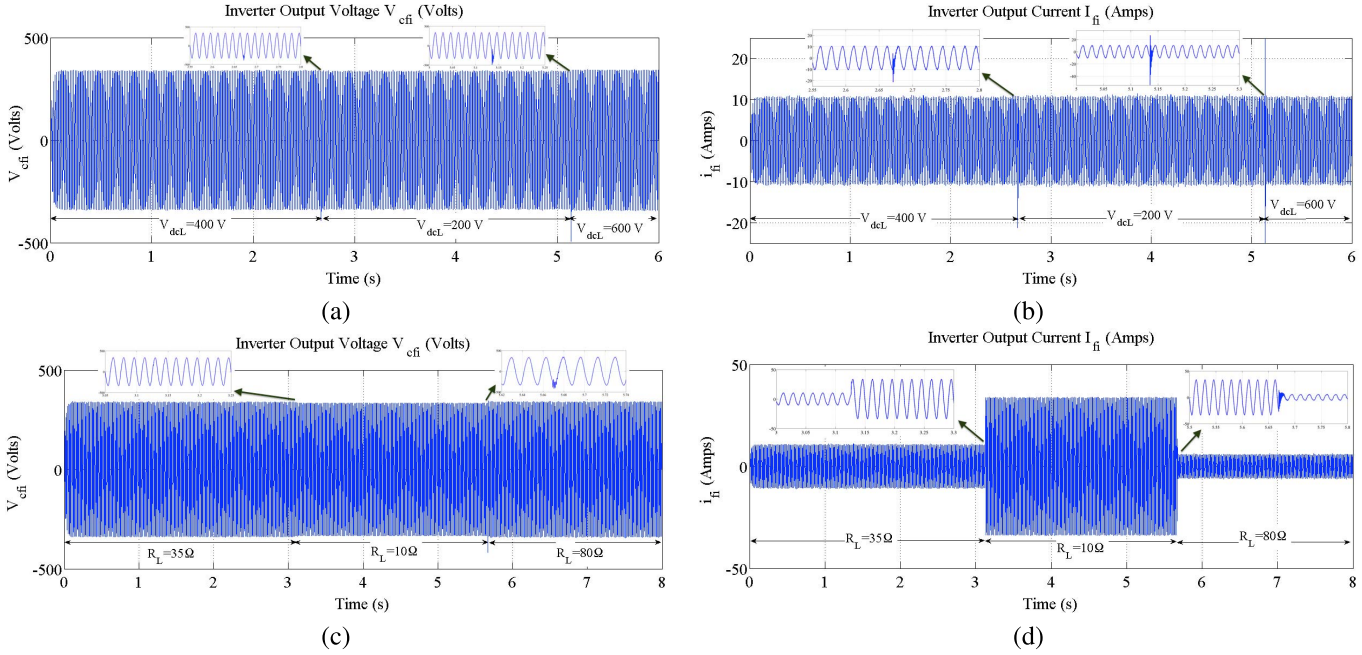

Fig. 15. HIL performance of Inverter stage 1 for input variations (a) output voltage and (b) output current and stage 2 for load variations (c) output voltage and (d) output current.

input grid voltage is varies from 7200 to 6400 V_{rms} at 1 s. The HVdc link output voltage under input variation is shown in Fig. 6(b), and we can see that output voltage is regulated at desired set value by controller action. For DAB, load resistance is considered as 38 Ω and input variation is given as 3800 V for 0 s $< t <$ 1 s and then changed to 4200 V for 1 s $< t <$ 2 s. The LVdc output voltage performance with and without controller is shown in Fig. 7(b).

In inverter, the load resistance is 35 Ω and input voltage is varies from 400 V for 0 s $< t <$ 1 s to 360 V for 1 s $< t <$ 2 s. Under this input variation, output voltage waveform is shown in Fig. 8(b) with and without controller action. Fig. 9 shows the constant duty ratio (S_i) applied for without controller action and duty ratio obtained by the IDA-PBC law. It shows that duty ratio is indeed varied with change in input to regulate output voltage at 230 V_{rms}.

Using the IDA-PBC control law, the operation of SST is not affected by source and load side disturbances, demonstrating system robustness. It also ascertains that the PBC is a design methodology, which can be used to stabilize the system and the response can be quite satisfactory.

V. Hardware-in-Loop Implementation

The model developed for SST was simulated in MATLAB/Simulink environment and the results were verified by porting plant model on Opal-RT while dSPACE used as controller.

A. Hardware-in-Loop Architecture

The proposed system is realized based on RT-LAB environment of Opal-RT, using RT toolbox and dSPACE Control desk environment in MATLAB/Simulink. The detailed structure of the HIL system used to validate the IDA-PBC control is illustrated in Fig. 10.

In HIL platforms, the Opal-RT module OP4500 mimics the plant (i.e., rectifier, DAB, and inverter stages of SST) and the dSPACE DS1104 acts as a controller. The RT-LAB simulator consists of two 3.33-GHz cores dedicated for parallel computation. OP4500 has 32-analog and 64-digital I/O channels to exchange data in real time [35]. The targets are equipped with Red Hat LINUX operating system and controlled via a Windows-based host computer using a TCP/IP connection. The interfacing between OP4500 and DS1104 is handled

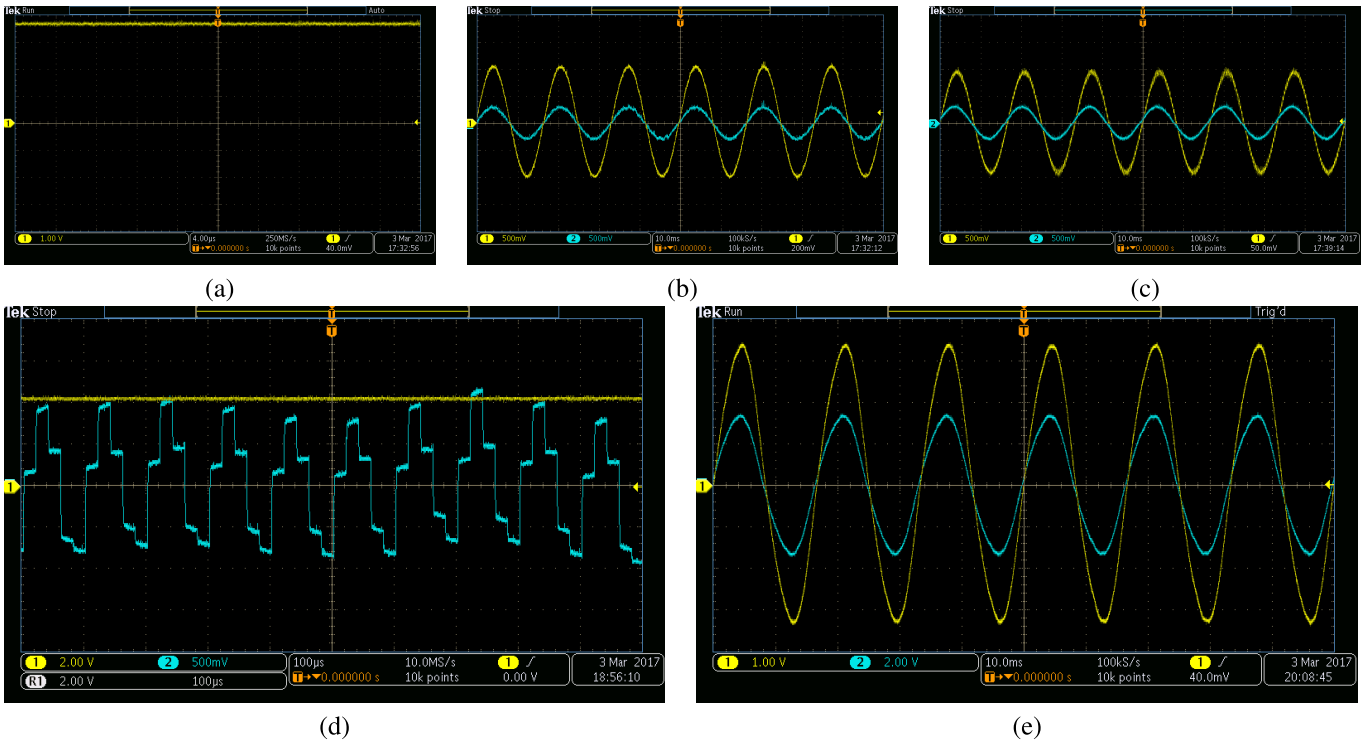

Fig. 16. Oscilloscope reading of all SST stages for load variations. (a) Rectifier output voltage. (b) Rectifier input voltage and current. (c) Rectifier input filter voltage and current. (d) DAB output voltage and transformer primary current. (e) Inverter output voltage and current. The yellow waveforms represent voltage, while the blue waveform is for current variable.

through fast Analog and Digital I/Os of OP4500 and DAC and ADC of DS1104.

The experimental setup required for HIL interface is demonstrated in Fig. 11. The detailed structure of this specific simulation will allow for real-time interaction through the GPIO of the field-programmable gate array (FPGA) DE2 board, which will accept inputs of output voltage reference ($\langle V_{\rm dcH}\rangle_0^d$), load resistance ($R_L$), and input voltage V_g. The DE2 board will compute output dc link voltage ($\langle V_{\rm dcH}\rangle$) and switching function μ_{r1} and μ_{r2}. The variables computed within the FPGA are using fixed-point notation, but are converted into 32-bit floating point for use in the DSP. The FPGA will communicate to a TI TMS320F240 DSP through the SPI [36]. The SPI core implemented within the FPGA configures the FPGA as the master device, while the DSP operates as the slave. By enabling the SPI data communication every $T = 20$ μs, the 32-bit floating-point variables ($\langle V_{\rm dcH}\rangle_0^d$, R_L, E, μ_{r1}, μ_{r2}, and $\langle V_{\rm dcH}\rangle_0$) have enough time to be transmitted at a SPI clock speed of 20 MHz. The time period of 20 μs gives enough computation time for the DSP to process the algorithm and to execute the control law. The DSP will also communicate to the PC running the dSPACE real-time environment through the dSPACE CLP1104 combined connector.

B. Hardware-in-Loop Experimental Results

The HIL is operating in real time and the results of the SST under the load and input variations via Opal-RT and dSPACE are verified. The simulation is performed for reference voltages ($\langle V_{\rm dcH}\rangle_0^d = 3800$ $V_{\rm dc}$ for rectifier, $\langle V_{\rm dcL}\rangle_0^d = 400$ $V_{\rm dc}$ for DAB, and $V_{\rm cfi} = 230$ $V_{\rm rms}$ for inverter). The HIL system is scaled down from the real-time simulated system using a voltage base of 1000 V, a current base of 100 A, and a load resistance base of 100 Ω, while the frequency remains constant.

The waveforms shown in Figs. 12–15 are the output waveforms from the RT Lab, which include rectifier, DAB, and inverter output. The results obtained from Opal-RT are compared with Simulink results and both are in close agreement. Fig. 16 shows the output voltage and current response for load variations as observed in oscilloscope for all three stages.

VI. Conclusion

This paper introduces the DP concept for the development of the PCPH model of SST. To explore the capabilities of nonlinear control techniques, IDA-PBC is applied at individual stages of SST. The passivity-based approach to nonlinear systems is more advisable than canceling nonlinearities and assigning high gain feedback, as it can be interpreted physically as an energy shaping technique and ensures the robustness properties of passive systems. An IDA-PBC control law has been designed for the load change and input voltage. The control law is defined in terms of phasor components of load current, load voltage, and input voltage. Experimental results demonstrate the feasibility of the designed controller. It is validated in the HIL framework using Opal-RT and dSPACE. It is found that the closed-loop system is robust to the load and input variations achieving unity power factor at input side and achieves desired output load voltage regulation.

APPENDIX A

1) Time-domain model of SST

$$L_g\frac{di_g}{dt} = V_g - V_{\rm fr} - R_g i_g \tag{71}$$
$$L_{\rm fr}\frac{di_f}{dt} = V_{\rm fr} - S_r V_{\rm dcH} - R_{\rm fr} i_{\rm fr} \tag{72}$$
$$C_{\rm fr}\frac{dV_{\rm fr}}{dt} = i_g - i_{\rm fr} \tag{73}$$
$$C_{\rm dcH}\frac{dV_{\rm dcH}}{dt} = S_r i_{\rm fr} - i_{tp} \tag{74}$$
$$L_t\frac{di_{\rm tp}}{dt} = S_{D1} V_{\rm dcH} - R_t i_{\rm tp} - S_{D2} V_{\rm dcL} \tag{75}$$
$$C_{\rm dcL}\frac{dV_{\rm dcL}}{dt} = S_{D2} i_{\rm tp} - (S_{i1} i_{\rm fi1}) - i_N \tag{76}$$
$$L_{\rm fi1}\frac{di_{\rm fi1}}{dt} = S_{i1} V_{\rm dcL} - R_{\rm fi1} i_{\rm fi1} - V_{\rm cfi1} \tag{77}$$
$$C_{\rm fi1}\frac{dV_{\rm cfi1}}{dt} = i_{\rm fi1} - \frac{V_{ci1}}{R_{L1}}. \tag{78}$$

2) DP-based model of SST

$$\frac{d\langle i_g\rangle_1^R}{dt} = \omega\langle i_g\rangle_1^I + \frac{1}{L_g}\big[\langle v_g\rangle_1^R - \langle v_{\rm fr}\rangle_1^R - R_g\langle i_g\rangle_1^R\big] \tag{79}$$
$$\frac{d\langle i_g\rangle_1^I}{dt} = -\omega\langle i_g\rangle_1^R + \frac{1}{L_g}\big[\langle v_g\rangle_1^I - \langle v_{\rm fr}\rangle_1^I - R_g\langle i_g\rangle_1^I\big] \tag{80}$$
$$\frac{d\langle i_{\rm fr}\rangle_1^R}{dt} = \omega\langle i_{\rm fr}\rangle_1^I + \frac{1}{L_{\rm fr}}\big[\langle v_{\rm fr}\rangle_1^R - \langle S_r\rangle_1^R\langle v_{\rm dcH}\rangle_0 - R_{\rm fr}\langle i_{\rm fr}\rangle_1^R\big] \tag{81}$$
$$\frac{d\langle i_{\rm fr}\rangle_1^I}{dt} = -\omega\langle i_{\rm fr}\rangle_1^R + \frac{1}{L_{\rm fr}}\big[\langle v_{\rm fr}\rangle_1^I - \langle S_r\rangle_1^I\langle v_{\rm dcH}\rangle_0 - R_{\rm fr}\langle i_{\rm fr}\rangle_1^I\big] \tag{82}$$
$$\frac{d\langle v_{\rm fr}\rangle_1^R}{dt} = \omega\langle v_{\rm fr}\rangle_1^I + \frac{1}{C_{\rm fr}}\big[\langle i_{\rm fr}\rangle_1^R - \langle i_g\rangle_1^R\big] \tag{83}$$
$$\frac{d\langle v_{\rm fr}\rangle_1^I}{dt} = -\omega\langle v_{\rm fr}\rangle_1^R + \frac{1}{C_{\rm fr}}\big[\langle i_{\rm fr}\rangle_1^I - \langle i_g\rangle_1^I\big] \tag{84}$$
$$\frac{d\langle v_{\rm dcH}\rangle_0}{dt} = \frac{1}{C_{\rm dcH}}2\big[\langle S_r\rangle_1^R\langle i_{\rm fr}\rangle_1^R + \langle S_r\rangle_1^I\langle i_{\rm fr}\rangle_1^I - \langle S_{D1}\rangle_1^I\langle i_{\rm tp}\rangle_1^I\big] \tag{85}$$
$$\frac{d\langle i_{\rm tp}\rangle_1^R}{dt} = \omega\langle i_{\rm tp}\rangle_1^I + \frac{1}{L_t}\big[\langle S_{D2}\rangle_1^R\langle v_{\rm dcH}\rangle_0 - R_t\langle i_{\rm tp}\rangle_1^R\big] \tag{86}$$
$$\frac{d\langle i_{\rm tp}\rangle_1^I}{dt} = -\omega\langle i_{\rm tp}\rangle_1^R + \frac{1}{L_t}\big[\langle S_{D1}\rangle_1^I\langle v_{\rm dcH}\rangle_0 + \langle S_{D2}\rangle\langle v_{\rm dcL}\rangle_0 - R_t\langle i_{\rm tp}\rangle_1^I\big] \tag{87}$$
$$\frac{d\langle v_{\rm dcL}\rangle_0}{dt} = \frac{2}{C_{\rm dcL}}\big[\langle S_{D2}\rangle_1^R\langle i_{\rm tp}\rangle_1^R + \langle S_{D2}\rangle_1^I\langle i_{\rm tp}\rangle_1^I - \langle S_{i1}\rangle_1^R\langle i_{\rm fi1}\rangle_1^R - \langle S_{i1}\rangle_1^I\langle i_{\rm fi1}\rangle_1^I\big] \tag{88}$$
$$\frac{d\langle i_{\rm fi1}\rangle_1^R}{dt} = \omega\langle i_{\rm fi1}\rangle_1^I + \frac{1}{L_{\rm fi1}}\big[\langle S_{i1}\rangle_1^R\langle v_{\rm dcL}\rangle_0 - \langle v_{\rm cfi1}\rangle_1^R - R_{\rm fi1}\langle i_{\rm fi1}\rangle_1^R\big] \tag{89}$$
$$\frac{d\langle i_{\rm fi1}\rangle_1^I}{dt} = -\omega\langle i_{\rm fi1}\rangle_1^R + \frac{1}{L_{\rm fi1}}\big[\langle S_{i1}\rangle_1^I\langle v_{\rm dcL}\rangle_0 - \langle v_{\rm cfi1}\rangle_1^I - R_{\rm fi1}\langle i_{\rm fi1}\rangle_1^I\big] \tag{90}$$

TABLE II
LIST OF VARIABLES CONSIDERED IN SST PCPH FORMATION

Rectifier stage	
λ_g, λ_{fr}	Flux of grid inductor L_g and filter inductor L_{fr} respectively
q_{cfr}, q_{dcH}	Charge of filter capacitor C_{fr} and HVDC capacitor C_{dcH} respectively
z_{dcH}	Transformed variable relating q_{dcH} as $z_{dcH} = q_{dcH}^2/2$
S_r	Switching function for rectifier
μ_r	Transformed variable relating S_r as $\mu_r = -S_r q_{dcH}$
x_{r1}, x_{r2}	Real and Imaginary parts of index-1 DP coefficient of λ_g
x_{r3}, x_{r4}	Real and Imaginary parts of index-1 DP coefficient of λ_{fr}
x_{r5}, x_{r6}	Real and Imaginary parts of index-1 DP coefficient of C_{fr}
x_{r7}	index-0 DP coefficient of z_{dcH}
μ_{r1}, μ_{r2}	Real and imaginary parts of index-1 DP coefficient of μ_r
J_r, R_r, H_r	Interconnection, Damping matrix, and Hamiltonian function
DAB stage	
λ_{tp}	Flux of transformer inductor L_t
q_{dcL}	Charge of LVDC capacitor C_{dcL}
z_{dcL}	Transformed variable relating q_{dcL} as $z_{dcL} = q_{dcL}^2/2$
S_{D2}	Switching function for DAB
μ_d	Transformed variable relating S_{D2} as $\mu_d = -S_{D2} q_{dcL}$
x_{d1}, x_{d2}	Real and Imaginary parts of index-1 DP coefficient of λ_{tp}
x_{d3}	index-0 DP coefficient of z_{dcL}
μ_{d1}, μ_{d2}	Real and imaginary parts of index-1 DP coefficient of μ_d
J_{DAB}, R_{DAB}, H_{DAB}	Interconnection, Damping matrix, and Hamiltonian function
λ_{fi}	Flux of filter inductor L_{fi}
q_{cfi}	Charge of filter capacitor C_{fi}
S_i	Switching function for inverter
x_{i1}, x_{i2}	Real and Imaginary parts of index-1 DP coefficient of λ_{fi}
x_{i3}, x_{i4}	Real and Imaginary parts of index-1 DP coefficient of q_{cfi}
μ_{i1}, μ_{i2}	Real and imaginary parts of index-1 DP coefficient of S_i
J_i, R_i, H_i	Interconnection, Damping matrix, and Hamiltonian function
Notations	
$*$	Steady state value
$\langle\,\rangle_1$	index-1 DP coefficient
$\langle\,\rangle_0$	index-0 DP coefficient

$$\frac{d\langle v_{\rm cfi1}\rangle_1^R}{dt} = \omega\langle v_{\rm cfi1}\rangle_1^I + \frac{1}{C_{\rm fi1}}\left[\langle i_{\rm fi1}\rangle_1^R - \left\langle\frac{v_{\rm cfi1}}{R_{L1}}\right\rangle_1^R\right] \tag{91}$$
$$\frac{d\langle v_{\rm cfi1}\rangle_1^I}{dt} = -\omega\langle v_{\rm cfi1}\rangle_1^R + \frac{1}{C_{\rm fi1}}\left[\langle i_{\rm fi1}\rangle_1^I - \left\langle\frac{v_{\rm cfi1}}{R_{L1}}\right\rangle_1^I\right]. \tag{92}$$

APPENDIX B

See Table II.

ACKNOWLEDGMENT

The authors would like to acknowledge the Future Renewable Electric Energy Distribution Management Center, NCSU, USA, and the Centre of Excellence in Complex and Nonlinear Dynamic Systems, VJTI, Matunga, Mumbai, India, under TEQIP-II (subcomponent 1.2.1) for their support.

REFERENCES

[1] A. Q. Huang, M. L. Crow, G. T. Heydt, J. P. Zheng, and S. J. Dale, "The future renewable electric energy delivery and management (FREEDM) system: The energy Internet," *Proc. IEEE*, vol. 99, no. 1, pp. 133–148, Jan. 2011.

[2] Z. Yu, R. Ayyanar, and I. Husain, "A detailed analytical model of a solid state transformer," in *Proc. IEEE Energy Convers. Congr. Expo. (ECCE)*, Sep. 2015, pp. 723–729.

[3] F. Wang, G. Wang, A. Huang, W. Yu, and X. Ni, "Design and operation of a 3.6 kV high performance solid state transformer based on 13 kV SiC MOSFET and JBS diode," in *Proc. IEEE Energy Convers. Congr. Expo. (ECCE)*, Sep. 2014, pp. 4553–4560.

[4] T. Zhao, J. Zeng, S. Bhattacharya, M. E. Baran, and A. Q. Huang, "An average model of solid state transformer for dynamic system simulation," in *Proc. IEEE Power Energy Soc. Gen. Meet.*, Jul. 2009, pp. 1–8.

[5] S. R. Sanders, J. M. Noworolski, X. Z. Liu, and G. C. Verghese, "Generalized averaging method for power conversion circuits," *IEEE Trans. Power Electron.*, vol. 6, no. 2, pp. 251–259, Apr. 1991.

[6] S. Almér, S. Mariéthoz, and M. Morari, "Dynamic phasor model predictive control of switched mode power converters," *IEEE Trans. Control Syst. Technol.*, vol. 23, no. 1, pp. 349–356, Jan. 2015.

[7] S. Bacha, I. Munteanu, and A. I. Bratcu, *Power Electronic Converters Modeling and Control: Advanced Textbooks in Control and Signal Processing*, vol. 454. London, U.K.: Springer, 2014.

[8] T. Yang, "Development of dynamic phasors for the modelling of aircraft electrical power systems," Ph.D. dissertation, Univ. Nottingham, Nottingham, U.K., 2013.

[9] A. Nagarajan and R. Ayyanar, "Dynamic phasor model of single-phase inverters for analysis and simulation of large power distribution systems," in *Proc. 4th IEEE Int. Symp. Power Electron. Distrib. Generat. Syst. (PEDG)*, Jul. 2013, pp. 1–6.

[10] H. Qin and J. W. Kimball, "Generalized average modeling of dual active bridge DC–DC converter," *IEEE Trans. Power Electron.*, vol. 27, no. 4, pp. 2078–2084, Apr. 2012.

[11] M. Parimi, M. Monika, M. Rane, S. Wagh, and A. Stankovic, "Dynamic phasor-based small-signal stability analysis and control of solid state transformer," in *Proc. 6th Int. Conf. Power Syst. (ICPS)*, Mar. 2016, pp. 1–6.

[12] D. S. Segaran, "Dynamic modelling and control of dual active bridge Bi-directional DC–DC converters for smart grid applications," Ph.D. dissertation, School Elect. Comput. Eng., RMIT Univ., Melbourne, VIC, Australia, 2013.

[13] H. Qin, "Dual active bridge converters in solid state transformers," Ph.D. dissertation, Missouri Univ. Sci. Technol., Rolla, MO, USA, 2012, paper 1914. [Online]. Available: http://scholarsmine.mst.edu/doctoral_dissertations/1914/

[14] D. G. Shah and M. L. Crow, "Stability design criteria for distribution systems with solid-state transformers," *IEEE Trans. Power Del.*, vol. 29, no. 6, pp. 2588–2595, Dec. 2014.

[15] M. Pérez, R. Ortega, and J. R. Espinoza, "Passivity-based PI control of switched power converters," *IEEE Trans. Control Syst. Technol.*, vol. 12, no. 6, pp. 881–890, Nov. 2004.

[16] R. Ortega and E. Garcia, "Energy-shaping stabilization of dynamical systems," Lab. Signaux Syst., Gif-sur-Yvette, France, Tech. Rep., 2003. [Online]. http://webpages.lss.supelec.fr/perso/ortega/slides-coursoSUPELEC-print-v1.pdf

[17] R. Ortega, A. J. van der Schaft, I. Mareels, and B. Maschke, "Putting energy back in control," *IEEE Control Syst.*, vol. 21, no. 2, pp. 18–33, Apr. 2001.

[18] J. Mendez, Y. Garcia, and M. T. Mata, "Three-phase power converter stabilization via total energy-shaping," in *Proc. 1st IEEE Conf. Ind. Electron. Appl.*, May 2006, pp. 1–6.

[19] C. Batlle, E. Fossas, R. Griñó, and S. Martínez, "Generalized state space averaging for port controlled Hamiltonian systems," in *Proc. 16th IFAC World Congr.*, 2005, pp. 836–841.

[20] G. Escobar, A. J. van der Schaft, and R. Ortega, "A Hamiltonian viewpoint in the modeling of switching power converters," *Automatica*, vol. 35, no. 3, pp. 445–452, 1999.

[21] C. Gaviria, E. Fossas, and R. Griñó, "Robust controller for a full-bridge rectifier using the IDA approach and GSSA modeling," *IEEE Trans. Circuits Syst. I, Reg. Papers*, vol. 52, no. 3, pp. 609–616, Mar. 2005.

[22] G. Escobar, D. Chevreau, R. Ortega, and E. Mendes, "An adaptive passivity-based controller for a unity power factor rectifier," *IEEE Trans. Control Syst. Technol.*, vol. 9, no. 4, pp. 637–644, Jul. 2001.

[23] A. Dòria-Cerezo, "Modeling, simulation and control of doubly-fed induction machine controlled by back-to-back converter," Ph.D. dissertation, Dept. Control Ind. Syst., Polytechnic Univ. Catalonia, Barcelona, Spain, 2006.

[24] H. Komurcugil, "Steady-state analysis and passivity-based control of single-phase PWM current-source inverters," *IEEE Trans. Ind. Electron.*, vol. 57, no. 3, pp. 1026–1030, Mar. 2010.

[25] H. Komurcugil, "Improved passivity-based control method and its robustness analysis for single-phase uninterruptible power supply inverters," *IET Power Electron.*, vol. 8, no. 8, pp. 1558–1570, 2015.

[26] R. Ortega and E. Garcia-Canseco, "Interconnection and damping assignment passivity-based control: A survey," *Eur. J. Control*, vol. 10, no. 5, pp. 432–450, 2004.

[27] C. Batlle, A. Dòria-Cerezo, and E. Fossas, "IDA-PBC controller for a bidirectional power flow full-bridge rectifier," in *Proc. 44th IEEE Conf. Decision Control Eur. Control Conf. (CDC-ECC)*, Dec. 2005, pp. 422–426.

[28] X. Mu, J. Wang, H. Xiang, Y. Ma, and D. Yang, "Study on a nonlinear control strategy for three-phase voltage sources PWM DC/AC inverter based on PCH model," in *Proc. IEEE Int. Conf. Electr. Mach. Syst. (ICEMS)*, Aug. 2011, pp. 1–4.

[29] M. Böttcher, J. Dannehl, and F. W. Fuchs, "Interconnection and damping assignment passivity-based current control of grid-connected PWM converter with LCL-filter," in *Proc. IEEE Int. Conf. Power Electron. Motion Control (EPE/PEMC)*, Sep. 2010, pp. T3–T20.

[30] D. Gerardo, E. Palacios, and V. Cárdenas, "Interconnection and damping passivity-based control applied to a single-phase voltage source inverter," in *Proc. IEEE 12th Int. Power Electron. Congr. (CIEP)*, Aug. 2010, pp. 229–234.

[31] R. Griñó, E. Fossas, and D. Biel, "Sliding mode control of a full-bridge unity power factor rectifier," in *Nonlinear and Adaptive Control*. Berlin, Germany: Springer, 2003, pp. 139–148.

[32] S. Almér and U. Jönsson, "Harmonic analysis of pulse-width modulated systems," *Automatica*, vol. 45, no. 4, pp. 851–862, 2009.

[33] G. Tadmor, "On approximate phasor models in dissipative bilinear systems," *IEEE Trans. Circuits Syst. I, Fundam. Theory Appl.*, vol. 49, no. 8, pp. 1167–1179, Aug. 2002.

[34] R. Ortega, A. van der Schaft, B. Maschke, and G. Escobar, "Interconnection and damping assignment passivity-based control of port-controlled Hamiltonian systems," *Automatica*, vol. 38, no. 4, pp. 585–596, 2002.

[35] OPAL-RT Technologies. *Powering Real-Time Simulation*. Acessed: Feb. 12, 2017. [Online]. Available: https://www.opal-rt.com/software-rt-lab/

[36] dSPACE. *DS1104 R&D Controller Board*. Acessed: Feb. 12, 2017. [Online]. Available: https://www.dspace.com/en/inc/home/products/hw/singbord/ds1104.cfm

Ragini V. Meshram received the B.E. degree in electrical engineering from the Government Engineering College, Aurangabad, India, in 2012, and the M.Tech. (specialization in control systems) degree from the Veermata Jijabai Technological Institute, Mumbai, India, in 2015, where she is currently pursuing the Ph.D. degree.

Her current research interests include nonlinear control design, switching power converters, electrical drives, and hybrid system control.

Monika Bhagwat received the B.E. degree in electrical engineering from R.D.V.V. University, Jabalpur, India, in 1994, and the M.Tech. degree in electrical engineering with specialization in control system from the Veermata Jijabai Technological Institute, Mumbai, India, in 2008, where she is currently pursuing the Ph.D. degree in electrical engineering.

Her current research interests include modeling and control of switched power converters in renewable energy integration.

Shubhangi Khade received the B.E. degree from Shivaji University, Kolhapur, India, in 2014, and the M.Tech. degree in power systems from the Veermata Jijabai Technological Institute, Mumbai, India, in 2016.

She is currently with the Trinity College of Engineering and Research, SPPU University, Pune, India. She has involved in the area of power system stability and nonlinear control system.

Sushama R. Wagh received the Ph.D. degree in electrical engineering from The University of Western Australia, Crawley, WA, Australia, in 2012.

From 2015 to 2016, she was with Tufts University, Medford, MA, USA. She is currently an Assistant Professor with the Veermata Jijabai Technological Institute, Mumbai, India. Her current research interests include power system stability and control.

Aleksandar M. Stanković (F'05) received the Ph.D. degree in electrical engineering from the Massachusetts Institute of Technology, Cambridge, MA, USA, in 1993.

From 1993 to 2010, he was with Northeastern University, Boston, MA, USA. He currently serves as an A.H. Howell Professor with Tufts University, Medford, MA, USA. He has held visiting positions at the United Technologies Research Center (sabbaticals in 2000 and 2007) and at L'Universite de Paris-Sud and Supelec (in 2004). He is a coeditor of a book series on power electronics and power systems for Springer.

Dr. Stanković is an Associate Editor of the IEEE TRANSACTIONS ON POWER SYSTEMS. He has previously served in the IEEE Transactions on Smart Grid on power systems and on control system technology in the same capacity, since 1996.

Navdeep M. Singh received the Ph.D. degree in electrical engineering from IIT Bombay, Mumbai, India, in 1990.

He is currently a Professor with the Veermata Jijabai Technological Institute, Mumbai. His current research interests include nonlinear control, geometric mechanics control, and control of underactuated mechanical systems.